ROYAL SOCIETY
OF CHEMISTRY

EDGE ARTICLE

Anthracene-functionalized dipolar glass copolymers as precursors for high-dielectric single-chain nanoparticles

Sebastian Bonardd,*[a] Jon Maiz, [ID][ab] Javier Maisueche,[a] Ester Verde-Sesto[ab] and José A. Pomposo [ID] *[abc]

Dipolar glass copolymers (DGCs) incorporating 9-anthrylmethyl methacrylate (**ANMA**) with dipolar monomers 2-(methylsulfonyl)ethyl methacrylate (**SO₂MA**) and 2-cyanoethyl methacrylate (**CNMA**) were synthesized *via* RAFT polymerization to develop high-performance dielectric materials with photo-responsive capabilities. Structural and spectroscopic analyses confirmed successful copolymer formation and anthracene incorporation, enabling ultraviolet (UV)-triggered functionalities. Thermal characterization revealed a significant increase in glass transition temperature ($\Delta T_g \approx$ +28 °C) compared to their homopolymer counterparts, despite a moderate reduction in thermal stability. Dielectric measurements demonstrated high permittivity ($\varepsilon_r' > 5.0$) and low loss factors across a broad temperature range, with distinct γ, β, and α relaxation processes identified. Upon UV irradiation, anthracene photodimerization enabled efficient intramolecular cross-linking under dilute, oxygen-free conditions, leading to the formation of discrete single-chain nanoparticles (SCNPs) as confirmed by combined UV-visible spectroscopy, size-exclusion chromatography, and dynamic light scattering analyses. We explore, for the first time, the use of programmable nanoscale architectures to develop a new generation of single-chain high-dielectric nanomaterials. These materials exhibit high permittivity, relatively low dielectric losses, and suitable thermal properties in terms of glass transition temperature. Our results show that the localized environment and the reduction of long-range entanglements, arising from the collapse of linear DGC precursors into single-chain nanoparticles, do not significantly alter the dielectric response of these entities. As a result, they provide efficient dielectric materials with potential applications in energy storage, flexible electronics, sensors, and smart materials.

1 Introduction

In recent years, polymer dielectrics have garnered considerable attention within the scientific community, driven by their critical role across a broad spectrum of electrical and electronic applications.[1] This growing interest is especially pronounced in the context of energy storage and conversion technologies, which are becoming increasingly vital in meeting the demands of a rapidly evolving global energy landscape shaped by the energy transition. Among these applications, capacitive systems have particularly benefited from the development of advanced polymer dielectric materials, enabling significant improvements in energy density, efficiency, and operational reliability. These advancements have facilitated the integration of polymer-based capacitors into a wide range of high-performance technologies, including pulsed power electronics, energy storage modules for renewable energy infrastructures, electric and hybrid transportation systems, aerospace platforms, soft robotics, and sensor networks.[2] The versatility and tunability of polymer dielectrics make them especially attractive for such applications, where lightweight, flexible, and high-dielectric-performance materials are essential. Beyond their role in emerging technologies, capacitors incorporating polymer dielectrics remain foundational components in conventional electronic circuits, ensuring the stable operation of everyday devices, from household appliances to critical medical equipment such as defibrillators. This dual relevance, spanning both cutting-edge and ubiquitous technologies, underscores the importance of continued research into the design, synthesis, and characterization of next-generation polymer dielectric materials.[3]

Among dielectric materials, polymers offer several advantages over their inorganic and organic-inorganic hybrid counterparts, positioning them as highly attractive candidates for capacitor fabrication.[4] Their intrinsic insulating nature, high

[a]Materials Physics Center (CFM-MPC), CSIC-UPV/EHU, Paseo Manuel de Lardizabal 5, 20018 Donostia, Spain

[b]IKERBASQUE - Basque Foundation for Science, Plaza Euskadi 5, 48009 Bilbao, Spain

[c]Department of Polymers and Advanced Materials: Physics, Chemistry and Technology, University of the Basque Country (UPV/EHU), Paseo Manuel de Lardizabal 3, 20800 Donostia, Spain

dielectric breakdown strength, mechanical robustness, ease of processing, low density, chemical resistance, synthetic tunability, and cost-effective manufacturing collectively contribute to their widespread adoption in dielectric applications.[5] Despite these merits, a major limitation of polymer dielectrics is their typically low relative dielectric constant (ε_r'), which generally falls within the range of 2.0 to 4.0.[6] This constraint is particularly significant given that both the capacitance ($C_P = \varepsilon_r'\varepsilon_0 A/d$) and the energy density ($U_e = \varepsilon_r'\varepsilon_0 E^2/2$) of a capacitor scale directly with (ε_r'), where ε_0 is the vacuum permittivity, A is the electrode area, d is the dielectric thickness, and E is the applied electric field. While both parameters ε_r' and E, influence a capacitor's energy storage capacity, E is more tightly constrained by the intrinsic nature of the material, making it difficult to enhance. In contrast, ε_r' is more tunable through strategies such as chemical modification of the polymer matrix. Consequently, enhancing the dielectric constant of polymers has become a central objective in the development of next-generation energy storage materials.[7]

In response, significant efforts have been devoted to the design of high-dielectric polymers, typically defined as systems exhibiting ε_r' values above 5.0, a benchmark regarded as the threshold to surpass in the field. Among the most promising strategies to achieve this goal is the dipolar glass polymer (DGP) concept, introduced by Lei Zhu in 2014.[6] DGPs have demonstrated the ability to combine elevated dielectric constants with low dissipative behavior, a critical attribute for efficient energy storage applications. A DGP, in its most fundamental form, must satisfy two key design criteria. First, the polymer backbone must incorporate covalently bound, small-sized functional groups with high dipole moments. Second, the material must be amorphous and exhibit a high glass transition temperature (T_g). The elevated ε_r' observed in DGPs arises from enhanced polarizability, attributed to the orientational motions of molecular dipoles within the free volume of the amorphous matrix when subjected to an external electric field. A high T_g is essential to suppress dissipative phenomena that become prominent as the polymer approaches or exceeds its glass transition. In the rubbery state, increased chain mobility facilitates long-range segmental relaxations and ionic conduction, both of which contribute to dielectric loss through molecular friction and the migration of ionic impurities. From a device perspective, operating near or above T_g can also compromise mechanical integrity, potentially leading to material flow and device failure. Therefore, the ideal DGP architecture enables molecular dipoles to retain sufficient mobility at sub-T_g temperatures, facilitated by localized, secondary relaxation processes, while the bulk matrix remains in a rigid, glassy state. This configuration supports efficient dipolar polarization across a broad temperature range while minimizing energy dissipation, thus achieving a high dielectric constant in conjunction with a low loss factor ($\tan(\delta)$).

Building on the foundational principles of DGPs, recent advances have identified sulfone-based moieties as among the most promising dipolar structures for designing high-performance DGPs. This has relegated nitrile groups, long considered the standard dipolar units in high-dielectric polymer design, to a secondary role following the emergence of sulfone chemistry. In a seminal study, Wei et al.[8] were the first to report a sulfonyl-functionalized DGP, achieving exceptional dielectric properties, with an ε_r' of 11.4 and a $\tan(\delta)$ of 0.02 at 1 Hz and 25 °C. Since then, the superiority of sulfonyl groups has been consistently demonstrated across a range of polymer systems, significantly surpassing the dielectric performance of conventional polymeric materials.[9–16] Currently, there is significant interest in the systematic investigation of sulfone-containing polymers, as evidenced by recent publications.[17–20] Experimental and theoretical analyses have shown that sulfone groups not only possess high intrinsic dipole moments but also exhibit enhanced mobility within polymer matrices compared to other dipolar structures. This dual advantage facilitates efficient dipolar orientation under an electric field, thereby boosting the overall polarizability and dielectric response of the material. Despite their advantages, incorporating sulfonyl functionalities into diverse polymer backbones presents synthetic challenges, often involving low-yielding reactions and the use of hazardous or difficult-to-handle reagents. In parallel, various strategies have been explored to achieve the high T_g values required for DGPs. These include the covalent attachment of bulky or rigid pendant groups,[21] the use of aromatic polymer backbones,[22] and the incorporation of rigid, twisted dipolar monomers to introduce intrinsic porosity,[23] each contributing to thermal stability while preserving dipolar mobility.

The concept of dipolar glass copolymers (DGCs) was recently introduced as a novel strategy to elevate T_g by incorporating monomers derived from high-T_g homopolymers, without compromising the dielectric performance of dipolar components (such as nitrile- or sulfone-based units).[24] This approach involves the integration of rigid dipolar co-monomers into the polymer backbone, thereby enhancing structural rigidity while maintaining sufficient polarizability. Building on this strategy, we report the synthesis and characterization of two new functional methacrylate-based DGCs bearing either nitrile or sulfone groups in combination with anthracene pendant units. We hypothesize that these copolymers will exhibit: (i) ε_r' values exceeding 5.0, due to the presence of strong dipoles from the nitrile or sulfone functionalities; (ii) T_g values above 100 °C, resulting from the bulkiness and rigidity of anthracene moieties and the inherently high T_g of the corresponding sulfone- and nitrile-based homopolymers; and (iii) light responsiveness *via* the well-known photodimerization reaction of anthracene units.[25] In relation to the latter, we investigate the dielectric properties of DGCs-based single-chain nanoparticles (SCNPs),[26] entities that hold potential for diverse applications and open new avenues for scientific discovery and technological innovation.[27–36] Indeed, we disclose single-chain dielectric nanomaterials with high $\varepsilon_r'(<7.0)$, (>7.0) relatively low dissipative character ($\tan(\delta) < 0.02$) and improved T_g values. These combined features strongly support the potential of this new class of SCNPs as promising candidates for organic electronics and energy storage applications, among others.

1.1. Materials

N,N'-Dicyclohexylcarbodiimide (DCC, $\geq$99%), 4-(dimethylamino)pyridine (DMAP, $\geq$99%), methacryloyl chloride (97%, contains monomethyl ether hydroquinone (MEHQ) as stabilizer), 3-hydroxypropanenitrile (97%), methacrylic acid (99%, containing 250 ppm MEHQ as inhibitor), 2-cyano-2-propyl benzodithioate (2CPBz, >97%), triethylamine (TEA, $\geq$99.5%) and deuterated chloroform (CDCl$_3$) (99.96 atom% D, containing 0.03% (v/v) tetramethylsilane) were all purchased from Sigma Aldrich (Merk). 2-(Methylsulfonyl)ethanol (98%) was purchased from Fluorochem. Azobisisobutyronitrile (AIBN, $\geq$99.5%) was purchased from Fluka and recrystallized before use. N,N-Dimethylformamide (DMF, $\geq$98.5%), dichloromethane (DCM, $\geq$99.5%), tetrahydrofuran (THF, $\geq$99.0%), n-hexane (n-Hex, $\geq$98.5%), acetone (Ace, $\geq$99.5%), chloroform (CHCl$_3$, $\geq$98.5%), ethyl acetate (EtOAc, $\geq$99.5%), and methanol (MeOH, $\geq$99.8%) were all purchased from Merck.

1.2. Synthesis of monomers

The synthesis of 2-(methylsulfonyl)ethyl methacrylate (SO$_2$MA), 2-cyanoethyl methacrylate (CNMA), and 9-anthrylmethyl methacrylate (ANMA), following synthetic procedures reported in the literature,[24,37,38] is depicted in Scheme 1.

1.2.1. 2-(Methylsulfonyl)ethyl methacrylate (SO$_2$MA). To a 100 mL round-bottom flask, 2-(methylsulfonyl)ethanol (2 g, 16.11 mmol) was added, and the flask was purged with dry N$_2$ for 15 min. Then, CHCl$_3$ (50 mL) and TEA (2.6 mL, 18.61 mmol) were added, and the flask was submerged in a cold acetone

Scheme 1 Synthesis of monomers: (A) 2-(Methylsulfonyl)ethyl methacrylate (SO$_2$MA). (B) 2-Cyanoethyl methacrylate (CNMA). (C) 9-Anthrylmethyl methacrylate (ANMA).

bath. Methacryloyl chloride (1.6 mL, 16.4 mmol) was then slowly added, and the reaction mixture was stirred for 12 h. Subsequently, an additional 0.3 mL of methacryloyl chloride was added, and the mixture was refluxed at 80 °C for 2 h. Next, water (50 mL) was added, and the reaction was stirred overnight. The mixture was then transferred to a separatory funnel and washed with three portions of saturated NaHCO$_3$ solution and two portions of brine. The organic phase was collected, dried over MgSO$_4$, filtered and concentrated under reduced pressure. The crude product was purified by column chromatography using EtOAc/n-hex (3/7) as the eluent, affording **SO$_2$MA** in a yield of 57.2% (1.77 g). ^{1}H and ^{13}C nuclear magnetic resonance (NMR) spectra, along with Fourier transform infrared (FTIR) spectra of **SO$_2$MA**, are provided in the SI (see Fig. S1–S3).

1.2.2. 2-Cyanoethyl methacrylate (CNMA). To a 250 mL round-bottom flask, DCC (6.92 g, 33.52 mmol) and DMAP (0.41 g, 3.33 mmol) were added. In a separate 15 mL vial, 3-hydroxypropanenitrile (2.0 mL, 28.39 mmol) and methacrylic acid (2.8 mL, 33.01 mmol) were combined and diluted with 10 mL of dry DCM. The round-bottom flask was purged with dry N$_2$ for 5 min, after which 50 mL of dry DCM were added to dissolve the solids. The flask was then placed in an ice bath, and the contents of the vial were injected dropwise. Approximately halfway through the addition, a white precipitate of dicyclohexylurea began to form, giving the solution a whitish appearance. The reaction was stirred for 24 h. Afterward, the mixture was filtered, and the solid was washed with cold DCM. The resulting yellow liquid was transferred to a separatory funnel and washed with three portions of 10% NaHCO$_3$ solution and two portions of brine. The organic phase was dried over MgSO$_4$, filtered, and the solvent removed via vacuum distillation. The crude product was purified by column chromatography using DCM as the eluent, affording **CNMA** as a yellow oil in 78.5% yield (3.10 g). ^{1}H NMR, ^{13}C NMR and FTIR spectra of **CNMA** are provided in the SI (Fig. S1–S3).

1.2.3. 9-Anthrylmethyl methacrylate (ANMA). In a 100 mL round-bottom glass equipped with a magnetic stirrer, DCC (2.3 g, 11.20 mmol) and DMAP (0.14 g, 1.20 mmol) were added and purged with nitrogen for 5 min. Then, 30 mL of THF were introduced, and the resulting solution was cooled to 0 °C. Separately, a solution of 9-anthracenemethanol (2.00 g, 9.30 mmol) and methacrylic acid (0.95 mL, 11.20 mmol) in 20 mL of THF was prepared and added dropwise to the first solution. The reaction mixture was stirred at room temperature for 24 h. After completion, the reaction was diluted with 50 mL of DCM and washed with brine (3 × 100 mL). The organic phase was dried with MgSO$_4$, filtered, and the solvent was removed through vacuum distillation. The obtained oil was purified by column chromatography using n-Hex/EtOAc (4/1) as eluent, affording a yellow, fluorescent solid in 82.1% yield (2.11 g). ^{1}H NMR, ^{13}C NMR, and FTIR spectra of **ANMA** are provided in the SI (Fig. S1–S3).

1.3. Synthesis of copolymers

The synthesis of the copolymers was carried out via reversible addition–fragmentation chain-transfer (RAFT)
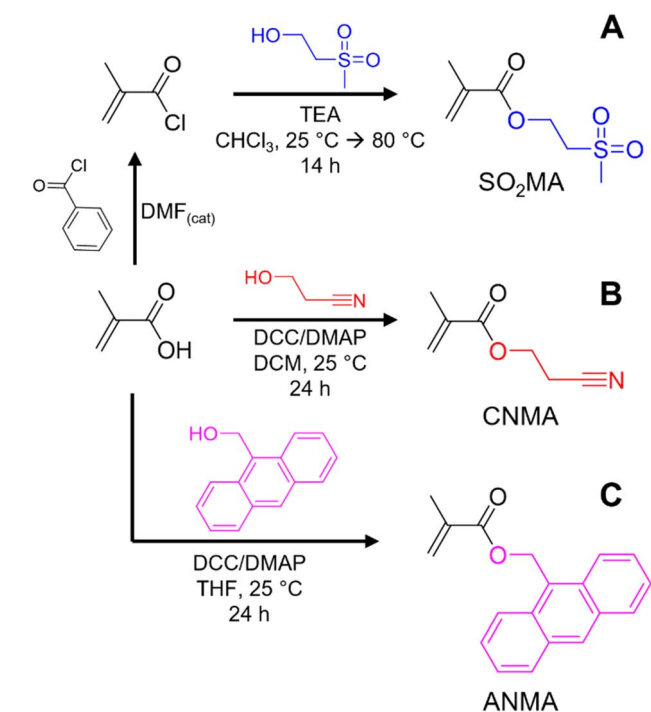
copolymerization using AIBN as the radical source and 2CPBz as the chain transfer agent (Scheme 2). The monomer mixtures were placed in a Schlenk tube equipped with a magnetic stirrer, degassed through five consecutive freeze–thaw cycles and subsequently filled with dry N_2. Polymerization was initiated by immersing the system in a preheated oil bath at 70 °C and allowed to proceed for 24 hours. Purification of the resulting copolymers was performed by precipitating the crude product from DMF into MeOH three times, followed by vacuum drying at 100 °C until a constant weight was achieved.

1.3.1. Poly(2-(methylsulfonyl)ethyl methacrylate-co-9-anthrylmethyl methacrylate), poly(SO₂MA-co-ANMA). Poly(SO₂-MA-co-ANMA) was prepared from 1.02 g of **SO₂MA**, 0.48 g of **ANMA**, 6.2 mg of 2CPBz, and 2.3 mg of AIBN solubilized in 1.5 mL of DMF. Yield: 75.3% (1.13 g). **SO₂MA** content (^{1}HNMR): 71.8 mol%. **ANMA** content (^{1}H NMR): 28.2 mol%. M_w (SEC): 49.2 kDa. Đ (SEC): 1.54.

1.3.2. Poly(2-cyanoethyl methacrylate-co-9-anthrylmethyl methacrylate), poly(CNMA-co-ANMA). Poly(CNMA-co-ANMA) was prepared from 0.91 g of **CNMA**, 0.59 g of **ANMA**, 6.2 mg of 2CPBz, and 2.3 mg of AIBN solubilized in 1.5 mL of DMF. Yield: 78.7% (1.18 g). **CNMA** content (^{1}H NMR): 71.1 mol%. **ANMA** content (^{1}H NMR): 28.9 mol%. M_w (SEC): 42.7 kDa. Đ (SEC): 1.38.

1.4. Synthesis of single-chain nanoparticles (SCNPs)

SCNPs were prepared by UV irradiation at 365 nm for 20 min of the precursor copolymer—**poly(SO₂MA-co-ANMA)** or **poly(CNMA-co-ANMA)**—in very diluted N_2 purged DMF solutions (2 mg mL^{-1}). SCNPs were recovered by precipitation in an excess of cold MeOH, subsequent centrifugation of the mixture to isolate the SCNPs. The obtained materials were soaked and stirred in Milli-Q water overnight, separated by centrifugation, and subsequently soaked and stirred in MeOH. After a second centrifugation, the SCNPs were dried in a vacuum oven at 80 °C for 72 h.

1.5. Characterization techniques

^{1}H NMR and ^{13}C NMR spectra were recorded on a Bruker Avance II-500 system using CDCl$_3$ and DMSO-d$_6$ as solvents for monomers and polymers, respectively. Fourier-transform infrared spectroscopy (FTIR) spectra were acquired using a Jasco FT/IR - 6300 spectrophotometer. Spectra were recorded in the 500 and 4000 cm^{-1} range after 34 scans in transmission mode with a resolution of 2 cm^{-1}, using samples prepared as KBr pellets.

Ultraviolet/visible (UV/Vis) spectroscopy measurements were carried out at 25 °C on an Agilent 8453A spectrophotometer equipped with a Peltier thermostatic cell holder (T-controller 89090A).

The molecular weight of the polymers was determined by size exclusion chromatography (SEC) using a Shimadzu Nexera 40 HPLC system equipped with a PolarGel-M guard column (50 × 7.5 mm) and a PolarGel-M analytical column (300 × 7.5 mm), both from Agilent. Detection was performed with a differential refractive index (dRI) detector (RID-20A, Shimadzu). A 0.1 wt% LiBr solution in DMF was used as the eluent at a flow rate of 1 mL min^{-1}. Polystyrene (PS) standards were used for conventional calibration.

Thermal characterization was performed using a simultaneous thermal analyzer (TG/DSC) Discovery SDT 650 and a differential scanning calorimeter (DSC) Discovery DSC 025, both from TA Instruments. Thermogravimetric analysis (TGA) was conducted from 25 °C to 900 °C at a heating rate of 10 °C min^{-1} under a nitrogen atmosphere. From the TGA curves, the degradation onset temperature (T_i), maximum weight loss rate temperature (T_{MD}), and residue percentage (R) were determined. T_i was defined as the temperature at which the sample had lost 5% of its initial mass. DSC analysis consisted of five consecutive steps: (i) dynamic heating from 25 °C to 200 °C at 20 °C min^{-1}, (ii) isothermal hold at 200 °C for 3 min, (iii) dynamic cooling from 200 °C to 0 °C at 20 °C min^{-1}, (iv) isothermal hold at 0 °C for 3 min, and finally, (v) dynamic heating from 0 °C to 200 °C at 10 °C min^{-1}. Glass transition temperatures (T_g) were determined from the inflection point in the final heating scan.

Broadband dielectric spectroscopy (BDS) was used to characterize the dielectric properties using a Novocontrol Alpha high-resolution analyzer with an applied AC voltage of 1.0 V. Isochronal spectra were collected from −150 °C to 150 °C over
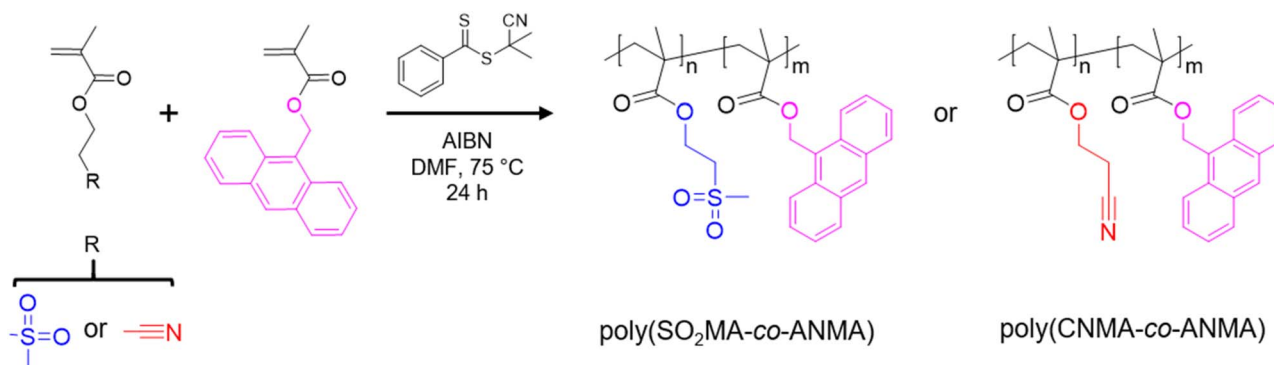
Scheme 2 Synthesis of copolymers: poly(2-(methylsulfonyl)ethyl methacrylate-co-9-anthrylmethyl methacrylate), **poly(SO₂MA-co-ANMA)**, and poly(2-cyanoethyl methacrylate-co-9-anthrylmethyl methacrylate), **poly(CNMA-co-ANMA)**.

a frequency range of $1–10^6$ Hz. For dielectric measurements, a specific amount of copolymer—or SCNPs—powder was first compressed into a disk at room temperature under a pressure of 10 tons. The resulting disk was then hot-pressed between two Teflon sheets at T_g + 30 °C under 1 bar for 45 min, producing a homogeneous, bubble-free film. This film was placed between two gold-coated electrodes of 10 mm and 20 mm in diameter, using the larger electrode as the bottom contact in a parallel-plate configuration. The film thickness was determined by measuring the peeled-off film after analysis. After their preparation, all samples were stored in a desiccator prior to measurement. The dielectric constant (ε'_r) was calculated using eqn (1):

$$\varepsilon'_r = \frac{C'_P d}{\varepsilon_0 \pi r^2} \tag{1}$$

where C'_P is the real part of the measured capacitance in the parallel configuration, d is the thickness of the polymer film, ε_0 is the vacuum permittivity (8.85×10^{-12} F m^{-1}) and r is the radius of the top electrode. Once ε'_r was calculated, the dielectric loss (ε''_r) was determined using the relation $\varepsilon''_r = \varepsilon'_r \tan(\delta)$, where $\tan(\delta)$ is the loss factor obtained directly from the experimental data.

Dynamic light scattering (DLS) measurements were conducted on a Zetasizer Nano (Malvern Instruments) to determine the hydrodynamic size distribution of the samples.

Photoirradiation experiments were performed at a wavelength of 365 nm using a Penn PhD photoreactor (Penn Photonics).

Intrinsic viscosity measurements were performed using an Ostwald viscometer.

2 Results and discussion

DGCs have recently emerged as a promising class of materials for high-performance polymer dielectrics.[24] This strategy aims to increase T_g, thereby expanding the operational temperature range while maintaining a low dielectric loss. The approach involves copolymerizing dipolar monomers, such as those bearing nitrile or sulfone functionalities, which impart excellent dielectric properties, with monomers that form high-T_g homopolymers. In this study, we present a further refinement of this concept by incorporating a functional monomer, 9-anthrylmethyl methacrylate. This monomer not only contributes to an elevated T_g but also introduces light responsiveness through photo-dimerization,[25] if needed. We explore the use of this property to pioneer the formation of DGCs-based SCNPs and innovative SCNPs-based high-dielectric materials.

2.1. Structural characterization of DGC linear precursors

Schemes 1 and 2 illustrate the synthetic routes used to prepare the monomers—**SO$_2$MA**, **CNMA** and **ANMA**—and copolymers—**poly(SO$_2$MA-co-ANMA)** and **poly(CNMA-co-ANMA)**—studied in this work. A complete characterization of the synthesized methacrylic monomers is provided in the SI (Fig. S1–S4). Copolymers of **SO$_2$MA** or **CNMA** with **ANMA** (25 mol% in the feed) were synthesized *via* RAFT polymerization. Table 1 presents the composition, molecular weight, and dispersity of **poly(SO$_2$MA-co-ANMA)** and **poly(CNMA-co-ANMA)**, as respectively (Fig. S5 and S8). It is worth noting that the obtained $Đ$ values, especially for the sulfone-containing system, are somewhat high for RAFT polymers. Nevertheless, similar trends have been reported for copolymers bearing sulfone pendant groups, with $Đ$ values typically ranging from 1.30 to 1.50.[24] While further optimization of the protocol (*e.g.*, avoiding extended reaction times to limit conversion) might reduce dispersity, the current results still allow for successful formation and characterization of the targeted SCNPs. Additionally, it has been demonstrated that the preparation of sulfonyl- and nitrile-containing DGPs by conventional radical polymerization yields $Đ$ values exceeding 2.0, emphasizing that even in these challenging systems, controlled radical polymerizations should be the preferred method.[8,17,18] Incorporating approximately 30% of the **ANMA** into the copolymers provides an effective balance, raising the T_g relative to neat **poly(SO$_2$MA)** or **poly(CNMA)**, while preserving the excellent dielectric properties imparted by the dipolar **SO$_2$MA** or **CNMA** monomers (see below). Additionally, cross-linkable monomer contents between 20 and 30 mol% have been shown to be ideal for promoting SCNP formation. ^{13}C NMR (Fig. S6) and FTIR spectroscopy (Fig. S7) further confirmed the presence of **SO$_2$MA** or **CNMA**, along with **ANMA**, in the copolymers. Due to the incorporation of anthracene moieties, UV-Vis spectroscopy revealed strong absorbance bands in the 300–400 nm range for both **poly(SO$_2$MA-co-ANMA)** and **poly(CNMA-co-ANMA)** (Fig. S9).
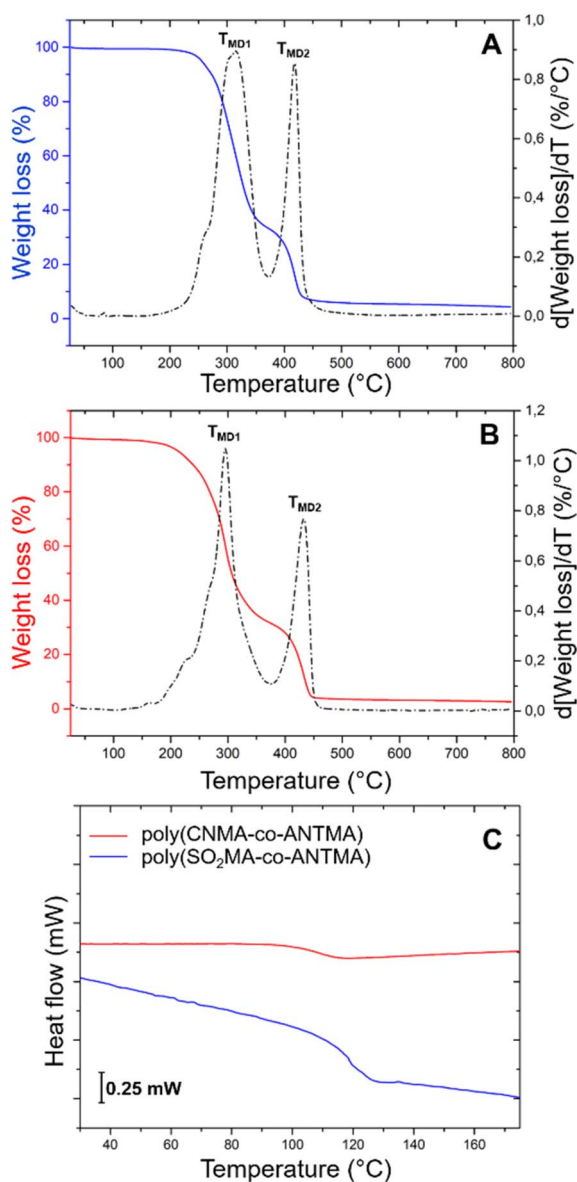
2.2. Thermal characterization of DGC linear precursors

The thermal stability of **poly(SO$_2$MA-co-ANMA)** and **poly(CNMA-co-ANMA)** was evaluated by TGA. The corresponding results are shown in Fig. 1A and B, from which thermal parameters listed in Table 2 were determined. Degradation of the copolymers occurs in two main steps, which presumably correspond to: (i) the cleavage of pendant groups (T_{MD1}), followed by (ii) the volatilization of species arising from random fragmentation and depolymerization of the copolymer backbone remaining after the first step (T_{MD2}). Incorporation of **ANMA** into the copolymers reduces the value of T_i by 30 °C and 42 °C compared to the **PSO$_2$MA** (T_i = 280 °C) and **PCNMA** (T_i = 265 °C) homopolymers, respectively. This reduction in T_i may be attributed to the more labile bond connecting the pendant group to the polymer backbone in **ANMA** units, which facilitates radical scission and subsequent thermally triggered depolymerization process, likely driven by the formation of more stable anthryl radical species. Conversely, due to the bulky nature of anthracene moieties, the presence of **ANMA** co-monomers increases the T_g of the copolymers by 28 °C in both cases (Fig. 1C), compared to **PSO$_2$MA** (T_g = 90 °C) and **PCNMA** (T_g = 81 °C) homopolymers, showing values of 118 °C and 109 °C for **poly(SO$_2$MA-co-ANMA)** and **poly(CNMA-co-ANMA)**, respectively. As expected, both DGC linear precursors were fully amorphous, with no signs of crystallization (Fig. 2).

Table 1 Monomer composition in feed mixtures and final copolymers, together with their weight average molecular weight (M_w) and dispersity (Đ)

Copolymer	ANMA (mol%) in the monomer mixture	ANMA (mol%) in the copolymer[a]	M_w (kDa)[b]	Đ[b]
poly(SO₂MA-*co*-ANMA)	25.0	28.2	49.2	1.54
poly(CNMA-*co*-ANMA)	25.0	28.9	42.7	1.38

[a] Determined by ^{1}H-NMR. [b] Determined by SEC.

Fig. 1 TGA and DTGA thermograms of poly(SO₂MA-*co*-ANMA) (A) and poly(CNMA-*co*-ANMA) (B) linear precursors. DSC traces recorded from last heating cycles (C).

2.3. Dielectric characterization of DGC linear precursors

Fig. 3 presents the isochronal curves of the ε_r', ε_r'' and tan(δ) for poly(SO₂MA-*co*-ANMA) and poly(CNMA-*co*-ANMA), illustrating the temperature dependence of dielectric properties at fixed frequencies. Starting with the ε_r' profiles (Fig. 3A and B), a continuous increase in this parameter is observed as the temperature rises. This well-documented behavior[39] is attributed to the sequential activation of distinct relaxation mechanisms, ranging from local and long-segmental motions to ion migration, as thermal energy become increasingly available to the system. However, the increase in ε_r' varies across specific temperature ranges. Both systems display a prominent step-like rise in ε_r' at low temperatures, between −150 and −50 °C, centered at −92 °C for poly(SO₂MA-*co*-ANMA) and −106 °C for poly(CNMA-*co*-ANMA). This behavior correlates with a distinct relaxation process, denoted as γ, observed in the ε_r'' curves (Fig. 3C and D). Based on previous studies, this γ−relaxation can be attributed to local reorientation of sulfone and nitrile dipoles in response to the applied electric field. These dipolar groups, while not the only contributors, play a primary role in polarization at these temperatures. As a result of the γ relaxation, ε_r' increases significantly in both materials, from 4.9 to 6.9 for poly(SO2MA-*co*-ANMA) and from 4.3 to 5.6 for poly(CNMA-*co*-ANMA), upon heating from −150 °C to −50 °C (at 1 Hz). These values already qualify both materials as high-dielectric polymers even at very low temperatures. Between approximately −50 °C and 75 °C, a more gradual increase in ε_r' is observed. This trend likely arises from the activation of additional dipolar entities, particularly the carbonyl groups in the ester linkages connecting the backbone to the pendant moieties. This relaxation process, designated as β, appears in both systems but is more pronounced in poly(SO₂MA-*co*-ANMA) (Fig. 3E). From this temperature range onward, dielectric properties at room temperature were assessed and are summarized in Table 3. Both copolymers show ε_r' values exceeding 5.0 while maintaining relatively low loss factors, confirming their suitability as low-dissipative, high-dielectric materials (see Table 3). At higher temperatures (>75 °C), both copolymers exhibit a steeper rise in ε_r', indicative of a more highly polarized state. However, this increase is accompanied by a sharp escalation in ε_r'' and tan(δ) (Fig. 3B, C, E, and F),

Table 2 Thermal degradation onset (T_i), maximum weight loss rate temperature (T_{max}) and residue percentage (R) of poly(SO₂MA-*co*-ANMA) and poly(CNMA-*co*-ANMA) as determined by TGA

Sample	T_i (°C)	T_{MD1} (°C)	T_{MD2} (°C)	R (%)
poly(SO₂MA-*co*-ANMA)	250	288	427	5.04
poly(CNMA-*co*-ANMA)	223	296	432	2.61

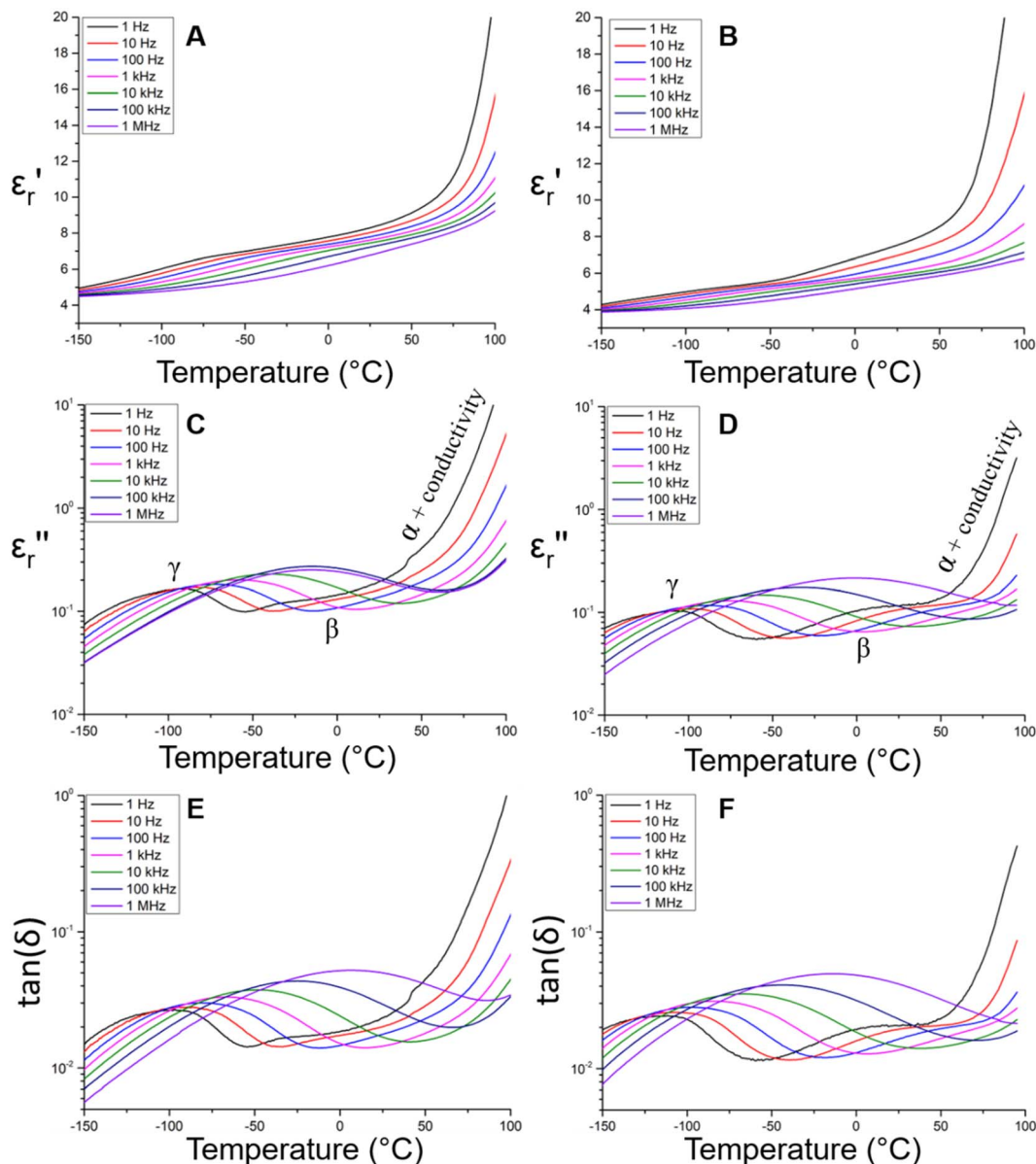Fig. 2   Isochronal representations of and tan(δ) for **poly(SO$_2$MA-co-ANMA)** (A, C and E) and **poly(CNMA-co-ANMA)** (B, D and F) linear precursors, enabling the evaluation, at fixed frequencies, of the polarization ability, dipolar relaxation behavior, and dissipative character of the materials as a function of temperature.

pointing to a significant rise in dielectric losses and dissipative behaviour. This transition marks the end of the DGP state and the onset of the paraelectric region, as the materials approach their T_gs. Near and above T_g, long-range segmental motions characteristic of the rubbery state become thermally activated, giving rise to the so-called α-relaxation process. This enhanced chain mobility, coupled with increased ionic conductivity, is largely attributed to the diffusion of residual ionic impurities inherently present in the polymer matrices. Consequently, the system displays a less desirable combination of high polarization and elevated dielectric loss at these temperatures.

Despite the high-temperature behaviour, the dielectric performance of both copolymers within the DGP region, between the γ/β relaxations and T_g, remains highly favourable.

In this regime, both materials exhibit strong polarization with minimal energy dissipation, validating their classification as high-dielectric polymers with promising potential for low-loss applications across a broad sub-T_g operating range.

2.4. Photo-induced formation of DGC-based SCNPs

Having confirmed the desirable dielectric behaviour on both DGCs, we next investigated their potential as precursors for SCNPs.[26–36] In this approach, we leveraged the well-established photodimerization of anthracene moieties[25] to induce the light-triggered intramolecular collapse of individual DGC chains under high dilution conditions.[40,41] This homo-functional strategy, which exploits anthracene as an internal
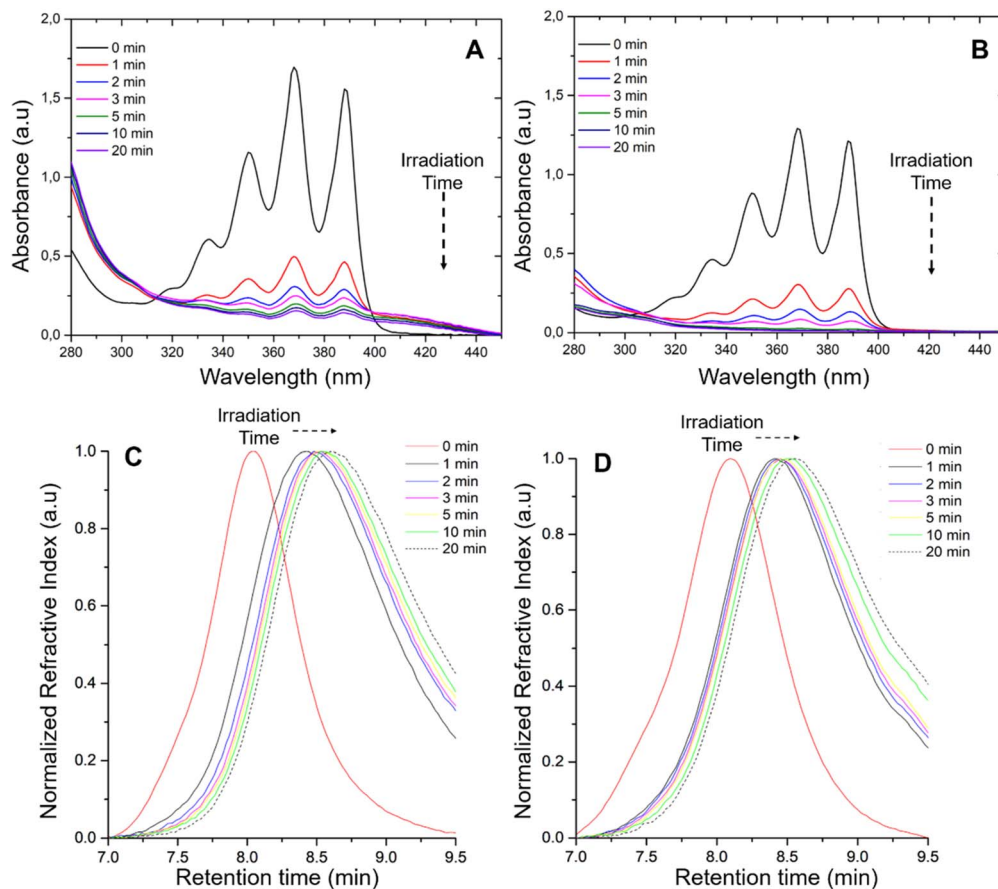
Fig. 3 UV-Vis spectra (top) and SEC traces (bottom) recorded for **poly(SO$_2$MA-*co*-ANMA)** (A and C) and **poly(CNMA-*co*-ANMA)** (B and D) solutions after photo-irradiation for different times (see text for details).

Table 3 Dielectric parameters of **poly(SO$_2$MA-*co*-ANMA)** and **poly(CNMA-*co*-ANMA)**

Sample	ε'_r (1 Hz)	ε'_r (1 kHz)	tan(δ) (1 Hz)	tan(δ) (1 kHz)
poly(SO$_2$MA-*co*-ANMA)	8.3	7.6	0.023	0.014
poly(CNMA-*co*-ANMA)	7.5	6.1	0.021	0.013

cross-linker, offers a clean and tuneable route to SCNP formation, avoiding the need for external cross-linking agents. To define the experimental conditions that favor intramolecular over intermolecular cross-linking, we first determined the coil overlap concentration[41] ($c*$) of both DGCs using intrinsic viscosity measurements in DMF. The intrinsic viscosities ([η]) of **poly(SO$_2$MA-*co*-ANMA)** and **poly(CNMA-*co*-ANMA)** were found to be 0.0178 and 0.0174 mL mg^{-1}, respectively. Applying the protocol reported by Vadillo *et al.*,[42] these values correspond to coil overlap concentrations of 82.2 and 84.2 mg mL^{-1}, respectively. Based on these results and in accordance with prior studies, we selected a working polymer concentration of 2 mg mL^{-1} for photoirradiation experiments, well below the $c*$ threshold, to ensure the formation of SCNPs though intrachain rather than interchain cross-linking.

The copolymer solutions were first purged with dry N$_2$ gas for 10 min, to eliminate dissolved oxygen, which can act as a dienophile in the well-known Diels–Alder-type photoperoxidation of anthracene moieties.[25] This side reaction deactivates anthracene units toward photodimerization, thereby hindering their participation in intrachain cross-linking and limiting SCNP formation. Following the degassing step, the solutions were exposed to UV light (365 nm) for defined time intervals and subsequently analysed by UV-Vis spectroscopy and SEC. As shown in Fig. 3A and B, UV-Vis spectra revealed a time-dependent decrease in the characteristic anthracene absorption bands for both copolymers, confirming successful photodimerization. This result is consistent with the loss of π-conjugation in anthracene upon cycloaddition, which significantly alters its optical properties. Notably, more than 50% of the initial absorbance intensity was lost within the first minute of irradiation, and the signal reached a plateau after approximately 20 min. Concurrently, SEC analysis of irradiated samples revealed a gradual shift towards higher retention times (Fig. 3C and D), indicating a reduction in hydrodynamic volume due to intrachain cross-linking and subsequent polymer chain collapse. Importantly, no signals corresponding to species with lower retention times were detected, ruling out the presence of intermolecularly cross-linked aggregates. To further validate the
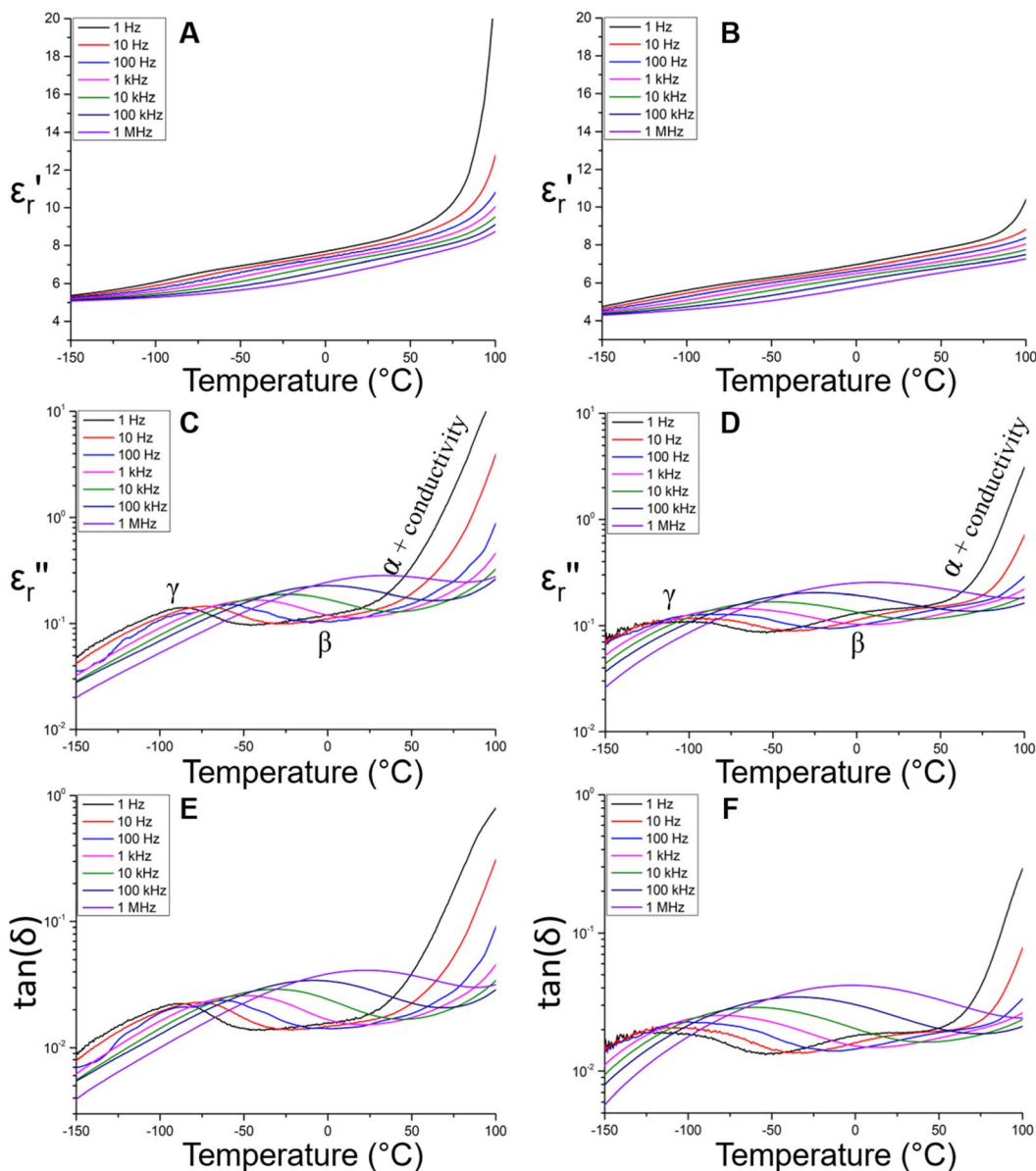
Fig. 4 Isochronal representations of ε_r', ε_r'' and tan(δ) for **poly(SO$_2$MA-co-ANMA)**-based SCNPs (A, C and E) and **poly(CNMA-co-ANMA)**-based SCNPs (B, D and F) enabling the evaluation, at fixed frequencies, of the polarization ability, dipolar relaxation behavior, and dissipative character of these materials as a function of temperature.

necessity of oxygen removal, control experiment conducted without N$_2$ purging showed significantly smaller shifts in SEC retention times under identical irradiation conditions (Fig. S10). This diminished response is attributed to the competitive photoperoxidation of anthracene, which reduces the number of available dimerizable units. To complement SEC data, DLS measurements performed before and after UV exposure confirmed a noticeable reduction in hydrodynamic diameter, providing additional evidence for the successful formation of discrete SCNPs (Fig. S11).

2.5. Dielectric properties of DGC-based SCNPs

After confirming the successful formation of SCNPs, we evaluated their dielectric properties under the same experimental

conditions used for their linear precursors. Specifically, we analysed the temperature dependence of ε_r', ε_r'' and tan(δ) at fixed frequencies for both **poly(SO$_2$MA-co-ANMA)**- and **poly(CNMA-co-ANMA)**-based SCNPs. The corresponding isochronal representations are presented in Fig. 4.

From Fig. 4, it is evident that the ε_r', ε_r'' and tan(δ) profiles recorded for both SCNP systems closely resemble those of their linear precursors. This observation indicates that collapsing the DGC precursors into SCNPs does not substantially alter the polarization ability, relaxational behaviour, and dissipative character of the materials. Accordingly, the discussion provided for the dielectric response of the linear precursors is also applicable here, as the increases in ε_r' over specific temperature intervals can be directly correlated with relaxation processes

identified in the ε_r'' profiles. Since the chemical nature of the dipoles remains unchanged during SCNP formation, the assignment of γ-transitions to sulfone and nitrile groups in **poly(SO₂MA-*co*-ANMA)**- and **poly(CNMA-*co*-ANMA)**-based SCNPs, respectively, and of β-relaxations to carbonyl structures, remains valid.

The persistence of these dipolar motions in the SCNPs is particularly important, as they sustain the polarization ability of the systems from very low temperatures up to room temperature, thereby determining the observed dielectric constant values. Consistent with this observation, the ε_r' values recorded for the SCNPs remain essentially unchanged, confirming that the ability of dipolar entities to contribute to the overall polarization of the system is preserved within the confined nanoparticle architecture. At room temperature, **poly(SO₂MA-*co*-ANMA)**- and **poly(CNMA-*co*-ANMA)**-based SCNPs exhibit ε_r' values of 8.1 and 7.4 at 1 Hz, and 7.6 and 6.8 at 1 kHz, respectively, well above the benchmark value of 5.0, thereby maintaining their classification as high-dielectric polymer materials, in line with their linear precursors. However, although the dipolar behaviour in the collapsed systems appears sufficient to match that of their linear precursors, a more detailed analysis of the γ-transitions reveals an interesting feature. When comparing γ-transitions between the linear and SCNP systems, it is observed that, at a fixed frequency, the maxima are shifted to higher temperatures in the collapsed architectures. For example, at 10 Hz, the maximum of this transition in the linear **poly(CNMA-*co*-ANMA)** precursor appears at −98 °C, whereas in its collapsed counterpart it is placed at −95 °C. This effect is even more pronounced for **poly(SO₂MA-*co*-ANMA)**, where, at 10 Hz, the γ-transitions for the linear and collapsed topologies are located at −82 °C and −73 °C, respectively. This means that sulfones and nitriles within SCNP entities require higher thermal energy to match the orientational motion rates observed in their linear precursors. A plausible explanation for this result is that the more collapsed environment provided by the particular topology of the SCNPs might enhance dipolar interactions.

On the other hand, both SCNP systems exhibit an increase in ε_r', ε_r'' and tan(δ) upon entering the high-temperature regime (>75 °C), which is also consistent with the observed dielectric response of their linear precursors. As previously discussed, this behaviour is attributed to the onset of α-relaxation, associated with the activation of long-segmental chain motions, which in turn facilitates ionic diffusion. The direct relationship between α-relaxation and T_g explains why the increase in these dielectric parameters occurs within the same temperature interval for precursors and SCNPs. Indeed, DSC scans recorded for **poly(SO₂MA-*co*-ANMA)**- and **poly(CNMA-*co*-ANMA)**-based SCNPs (Fig. S12) reveal T_g values of 119 °C and 111 °C, respectively, which are very close to those of their linear precursors. These results are consistent with previous reports showing that the collapse of polymer chains into SCNPs is generally accompanied by a slight increase in T_g.[43,44] Notably, the already low dissipative character of the linear precursors is retained in their SCNP counterparts, with further improvements observed in the recorded tan(δ) values. In this context, at room temperature,

poly(SO₂MA-*co*-ANMA)- and **poly(CNMA-*co*-ANMA)**-based SCNPs exhibit tan(δ) values of 0.018 and 0.019 at 1 Hz, and 0.015 and 0.016 at 1 kHz, respectively. Overall, the temperature dependence of dielectric parameters recorded for SCNPs follows trends comparable to those observed for the parent copolymers, suggesting that the reduction of long-range entanglements in the bulk SCNPs material has only a minor impact on the overall dielectric response. This observation highlights the robustness of the dielectric properties against topological reorganization.

3 Conclusions

Dipolar glass copolymers (DGCs) incorporating 9-anthrylmethyl methacrylate (**ANMA**) were successfully synthesized *via* RAFT polymerization with the dipolar monomers **SO₂MA** and **CNMA**. Structural characterization confirmed effective incorporation of ∼30 mol% **ANMA**, providing an optimal trade-off between enhanced thermal and maintained dielectric performance. The presence of anthracene units was validated by strong UV-Vis absorption in the 300–400 nm range, enabling photo-responsiveness. Thermal analysis revealed a moderate reduction in the onset degradation temperature due to **ANMA** incorporation, yet a notable increase in glass transition temperature ($\Delta T_g \approx$ +28 °C), with both copolymers remaining fully amorphous, an advantageous trait for dielectric materials.

Dielectric spectroscopy confirmed the high performance of both DGCs, with ε' values exceeding 5.0 at room temperature and low dielectric losses. Three well-resolved relaxation processes (γ, β, and α) were identified: γ attributed to local motions of sulfone or nitrile dipoles, β to ester carbonyl dynamics, and α, to long-range segmental motion near T_g. Although α-relaxation marked the onset of increased dielectric loss at elevated temperatures, the materials maintained high dielectric strength and stability across a broad operational range.

The anthracene functionality was further leveraged to induce photo-triggered intramolecular cross-linking *via* UV (365 nm) irradiation under dilute, oxygen-free conditions. Viscosity-based determination of coil overlap concentration ensured dilute conditions for single-chain collapse. Time-resolved UV-Vis and SEC analyses confirmed efficient anthracene dimerization and the progressive reduction of hydrodynamic size, without evidence of intramolecular aggregation process. DLS measurements further corroborated the formation of discrete single-chain nanoparticles (SCNPs). Notably, oxygen-free conditions were essential to suppress anthracene photo-peroxidation and ensure efficient, selective collapse.

The dielectric properties of **poly(SO₂MA-*co*-ANMA)**- and **poly(CNMA-*co*-ANMA)**-based SCNPs exhibit a temperature dependence comparable to their linear DGC precursors. This indicates that the collapse into a nanoparticle topology and the consequent reduction of long-range chain entanglements have a negligible effect on the overall dielectric response of these SCNPs in bulk. Thus, obtained SCNPs kept the high-dielectric ($\varepsilon_r' > 7.0$) and low dissipative (tan(δ) < 0.02) status of their linear precursors. The robustness of these properties against

such significant topological reorganization is a key finding, where the localized polar environment within the SCNPs does not alter significantly the polarization ability of the system. Consequently, the intramolecular collapse of DGC linear precursors into SCNPs offers an effective approach for creating advanced dielectric materials without sacrificing performance. Since ϵ_r' plays a central role in a wide range of physical and chemical phenomena, the distinct dielectric features imparted to these DGC-based SCNPs highlight their untapped potential to expand application possibilities and emphasize their importance as promising targets for materials innovation. Overall, this work provides a versatile platform for designing next-generation nanomaterials for use in organic electronics, energy storage, and more, while also opening new pathways to explore different DGC structures and alternative collapse strategies.

Author contributions

Conflicts of interest

There are no conflicts to declare.

Data availability

Data supporting of this article has been supplied within the SI File. Supplementary information: Fig. S1–S11. See DOI: https://doi.org/10.1039/d5sc05454k.

Acknowledgements

References

1 M. Yang, M. Guo, E. Xu, W. Ren, D. Wang, S. Li, S. Zhang, C.-W. Nan and Y. Shen, *Nat. Nanotechnol.*, 2024, **19**, 588.

2 H. Li, Y. Zhou, Y. Liu, L. Li, Y. Liu and Q. Wang, *Chem. Soc. Rev.*, 2021, **50**, 6369.

3 I. O. Oladele, S. O. Adelani, A. S. Taiwo, I. M. Akinbamiyorin, O. F. Olanrewaju and A. O. Orisawayi, *RSC Adv.*, 2025, **15**, 7509.

4 J.-W. Zha, M.-S. Zheng, B.-H. Fan and Z.-M. Dang, *Nano Energy*, 2021, **89**, 106438.

5 S. Wang, C. Yang, X. Li, H. Jia, S. Liu, X. Liu, T. Minari and Q. Sun, *J. Mater. Chem. C*, 2022, **10**, 6196.

6 L. Zhu, *J. Phys. Chem. Lett.*, 2014, **5**, 3677.

7 E. Baer and L. Zhu, *Macromolecules*, 2017, **50**, 2239.

8 J. Wei, Z. Zhang, J.-K. Tseng, I. Treufeld, X. Liu, M. H. Litt and L. Zhu, *ACS Appl. Mater. Interfaces*, 2015, **7**, 5248.

9 J. Wei, T. Ju, W. Huang, J. Song, N. Yan, F. Wang, A. Shen, Z. Li and L. Zhu, *Polymer*, 2019, **178**, 121688.

10 W. Huang, T. Ju, R. Li, Y. Duan, Y. Duan, J. Wei and L. Zhu, *Adv. Electron. Mater.*, 2023, **9**, 2200414.

11 D. Wu, X. Zhao, X. Li, J. Dong and Q. Zhang, *Polymer*, 2022, **256**, 125221.

12 Z. Zhang, D. H. Wang, M. H. Litt, L. S. Tan and L. Zhu, *Angew. Chem.*, 2018, **130**, 1544.

13 Y.-F. Zhu, Z. Zhang, M. H. Litt and L. Zhu, *Macromolecules*, 2018, **51**, 6257.

14 S. J. Dünki, E. Cuervo-Reyes and D. M. Opris, *Polym. Chem.*, 2017, **8**, 715.

15 Y. Sheima, T. R. Venkatesan, H. Frauenrath and D. M. Opris, *J. Mater. Chem. C*, 2023, **11**, 7367.

16 Y. Liang, J. Xu, W. Sun, T. Li, C. Dong, Y. Zhou, H. Zheng, Y. Cheng and L. Zhang, *Chem. Eng. J.*, 2024, **484**, 149458.

17 S. Bonardd, A. Alegria, C. Saldias, A. Leiva and G. Kortaberria, *ACS Appl. Mater. Interfaces*, 2018, **10**, 38476.

18 S. Bonardd, C. Saldías, Á. Leiva, D. Díaz Díaz and G. Kortaberria, *Polymers*, 2021, **13**, 317.

19 S. Bonardd, Á. Alegria, O. Ramirez, C. Saldías, Á. Leiva and G. Kortaberria, *React. Funct. Polym.*, 2019, **140**, 1.

20 S. Bonardd, J. Maiz, A. Alegría, J. A. Pomposo, E. V. Sesto, G. Kortaberria and D. D. Díaz, *React. Funct. Polym.*, 2024, **196**, 105842.

21 G. R. Davies, H. V. S. A. Hubbard, I. M. Ward, W. J. Feast, V. C. Gibson, E. Khosravi and E. L. Marshall, *Polymer*, 1995, **36**, 235.

22 I. Treufeld, D. H. Wang, B. A. Kurish, L. S. Tan and L. Zhu, *J. Mater. Chem. A*, 2014, **2**, 20683.

23 Z. Zhang, J. Zheng, K. Premasiri, M.-H. Kwok, Q. Li, R. Li, S. Zhang, M. H. Litt, X. P. Gao and L. Zhu, *Mater. Horiz.*, 2020, **7**, 592.

24 S. Bonardd, Á. Alegría, J. Maiz and D. D. Díaz, *Mater. Today Chem.*, 2024, **40**, 102268.

25 H. Bouas-Laurent, A. Castellan, J.-P. Desvergne and R. Lapouyade, *Chem. Soc. Rev.*, 2000, **29**, 43.

26 *Single-Chain Polymer Nanoparticles: Synthesis, Characterization, Simulations and Applications*, ed. J. A. Pomposo, Wiley-VCH, Weinheim, 2017.

27 E. Blasco, B. T. Tuten, H. Frisch, A. Lederer and C. Barner-Kowollik, *Polym. Chem.*, 2017, **8**, 5845.

28 P. H. Maag, F. Feist, H. Frisch, P. W. Roesky and C. Barner-Kowollik, *Chem. Sci.*, 2024, **15**, 5218.

29 J. P. Wang, R. Wang, Y. W. Gu, A. Sourakov, B. D. Olsen and J. A. Johnson, *Chem. Sci.*, 2019, **10**, 5332.

30 Y. J. Chen, Z. Y. Hu, Z. G. Shen, X. Q. Xue and H. T. Pu, *Chem. Sci.*, 2024, **15**, 17590.

31 S. Gillhuber, J. O. Holloway, K. Mundsinger, J. A. Kammerer, J. R. Harmer, H. Frisch, C. Barner-Kowollik and P. W. Roesky, *Chem. Sci.*, 2024, **15**, 15280.

32 M. A. M. Alqarni, C. Waldron, G. Yilmaz and C. R. Becer, *Macromol. Rapid Commun.*, 2021, **42**, 2100035.

33 K. Mundsinger, A. Izuagbe, B. T. Tuten, P. W. Roesky and C. Barner-Kowollik, *Angew. Chem., Int. Ed.*, 2024, **63**, e202311734.

34 H. Kalmer, F. Sbordone, J. McMurtrie, C. Nitsche and H. Frisch, *Macromol. Rapid Commun.*, 2025, **46**, 2400591.

35 P. J. M. Stals, C. Y. Cheng, L. van Beek, A. C. Wauters, A. R. A. Palmans, S. G. Han and E. W. Meijer, *Chem. Sci.*, 2016, **7**, 2011.

36 L. L. Deng, A. R. Olea, A. Ortiz-Perez, B. B. Sun, J. H. Wang, S. Pujals, A. R. A. Palmans and L. Albertazzi, *Small Methods*, 2024, **8**, 2301072.

37 C. S. Marvel, W. S. Anderson, B. H. Weil, E. E. Ryder, H. K. Inskip, M. Passer, W. K. Taft and G. B. Labbe, *Ind. Eng. Chem.*, 1955, **47**, 344.

38 D. Neugebauer, D. Charasim, A. Swinarew, A. Stolarzewicz, M. Krompiec, H. Janeczek, J. Simokaitiene and J. V. Gražulevičius, *Polym. J.*, 2011, **43**, 448.

39 Q.-K. Feng, S.-L. Zhong, J.-Y. Pei, Y. Zhao, D.-L. Zhang, D.-F. Liu, Y.-X. Zhang and Z.-M. Dang, *Chem. Rev.*, 2022, **122**, 3820.

40 P. G. Frank, B. T. Tuten, A. Prasher, D. Chao and E. B. Berda, *Macromol. Rapid Commun.*, 2014, **35**, 249.

41 T. Chidanguro, D. R. Blank, A. Garrett, C. M. Reese, J. M. Schekman, X. Yu, D. L. Patton, N. Ayres and Y. C. Simon, *Dalton Trans.*, 2018, **47**, 8663.

42 D. C. Vadillo, W. Mathues and C. Clasen, *Rheol. Acta*, 2012, **51**, 755.

43 J. Maiz, E. Verde-Sesto, I. Asenjo-Sanz, L. Mangin-Thro, B. Frick, J. A. Pomposo, A. Arbe and J. Colmenero, *Macromolecules*, 2022, **55**, 2320.

44 M. Gomez-Menendez, I. Asenjo-Sanz, E. Verde-Sesto, A. Iturrospe, J. A. Pomposo, A. Arbe and J. Maiz, *Polymer*, 2025, **335**, 128759.